Appl. Phys. A 90, 105–112 (2008)
DOI: 10.1007/s00339-007-4322-0

Applied Physics A
Materials Science & Processing

J.L. PAN✉
J.E. MCMANIS
M. GUPTA
M.P. YOUNG
J.M. WOODALL

Novel deep centers for high-performance optical materials

Yale University, P.O. Box 208284, New Haven, CT 06520-8284, USA

Received: 16 August 2007/Accepted: 28 September 2007
Published online: 25 October 2007 • © Springer-Verlag 2007

ABSTRACT Materials exhibiting strong optical emission also exhibit strong absorption at the same wavelengths because both emission and absorption are governed by the same optical dipole and density-of-states. Laser action requires a carrier injection large enough for emission to exceed absorption at laser wavelengths. Thus, strong self-absorption at luminescent wavelengths raises the operating current of LEDs, lasers, and optical amplifiers. Here we demonstrate that, contrary to conventional expectations, materials designed with novel deep centers achieve surprisingly large optical emission while, simultaneously, the inverse process of optical absorption remains very small. A striking consequence is that materials designed with our novel deep centers achieve transparency at a carrier injection which is four-orders-of-magnitude lower than in all technologically important semiconductors. Simultaneously, and surprisingly, our novel deep centers in GaAs achieve an optical gain, Einstein B coefficient, and radiative efficiency significantly larger than in direct-band-gap materials at 1.3–1.5 μm. We engineered this dramatic reduction of the injection to achieve transparency while retaining strong optical emission in our novel material by making use of a Franck–Condon shift of absorption away from luminescent wavelengths.

PACS 71.55.Eq; 71.55.-i; 78.67.-n; 81.10.-h; 85.60.Jb

1 Introduction

Materials exhibiting strong optical emission also exhibit strong absorption at the same wavelengths because both emission and absorption are governed by the same optical dipole and density-of-states. In 1961, Bernard and Duraffourg [1–3] showed that laser action requires an injection large enough for emission to exceed absorption at laser wavelengths. Thus, strong self-absorption at luminescent wavelengths raises the operating current of LEDs, lasers, and optical amplifiers. Since the 1960s [3–7], LEDs and lasers have utilized direct-band-gap transitions, which require [3, 8, 9] a sizable injection ($\sim 1\,\mathrm{kA/cm^2}$ or $10^{18}\,\mathrm{cm^{-3}}$) to achieve transparency. Here we demonstrate that, contrary to conventional expectations, materials designed with novel deep centers achieve surprisingly large optical emission while, simultaneously, the inverse process of optical absorption remains small. A striking consequence is that materials designed with our deep centers achieve transparency at an injection which is four-orders-of-magnitude lower than in all technologically important semiconductors. Simultaneously, and surprisingly, our novel deep centers achieve optical emission significantly larger than in direct-band-gap materials. We show that our deep centers in GaAs achieve an Einstein B coefficient eight times the B coefficient in direct-band-gap semiconductors (e.g. InGaAsP). Our deep centers in GaAs also achieved a total radiative output larger than from high-quality InGaAs-quantum-wells-on-InP, an internal efficiency of over 90% for light emission at 1.3–1.5 μm, and net optical gains[1] of $250\,\mathrm{cm^{-1}}$. (At 1.3–1.5 μm wavelengths, conventional direct-gap materials have a lower total radiative output and lower radiative efficiency ($< 50\%$ at injections near threshold) than our novel material because of fundamental Auger processes [3] as well as the detrimental effects of lattice-mismatched growth.) This net optical gain[1] in our novel material is 18 times and 10 times, respectively, the net gain required for laser action in quantum dots [10] and InGaAsN [11]. We engineered this large reduction of the injection to achieve transparency while retaining strong optical emission in our novel material by utilizing a Franck–Condon spectral shift of absorption away from luminescence. This Franck–Condon shift results in a self-absorption ($\sim 3.6\,\mathrm{cm^{-1}}$) at luminescent wavelengths which is much smaller than the $10^4\,\mathrm{cm^{-1}}$ typical of direct-band-gap semiconductors. Our new material is found to be an ideal four-level system, with a large Einstein B coefficient and femtosecond depopulation of the lower state of optical emission. Moreover, our deep centers showed more temperature-insensitive luminescence than InGaAs or InGaAsN, even for a rise of 90 °C.

✉ Fax: +1-203-432-6420, E-mail: janet.pan@yale.edu

[1] Our measured $250\,\mathrm{cm^{-1}}$ of net optical gain corresponds to the $\Gamma g - \alpha$ term from the literature [3], where Γ is the confinement factor, g is the material gain of the active layer, and α is the internal loss. For comparison, laser action in quantum dots [10] and InGaAsN [11] is achieved with net gains, $\Gamma g - \alpha$, of $14\,\mathrm{cm^{-1}}$ and $25\,\mathrm{cm^{-1}}$, respectively. Our measured $250\,\mathrm{cm^{-1}}$ gain compares very favorably with the best values in quantum dots [10] and InGaAsN [11], because the latter are limited by the detrimental effects of lattice-mismatched growth.

Thus, our novel material enables new 1.3–1.5 μm wavelengths directly from GaAs without strained-lattice epitaxy.

We have developed a new growth technique where a high n-doping is used to thermodynamically favor the formation of large concentrations of compensating deep acceptors. Though deep centers in n-GaAs have been known since the 1960s [12–21], our material is novel because n-GaAs is not usually designed to retain large concentrations of compensating acceptors. Whereas deep centers in n-GaAs typically exhibit radiative efficiencies of $\sim 1\%$ [22–24], we find the radiative efficiency of our deep centers to be over 90%. Our growth conditions favor the formation of deep levels below mid gap, and not above mid gap. This allows the formation of a pseudo band gap between the conduction band and mid gap (Fig. 1a). The absence of states within this pseudo band gap makes the radiative efficiency large. (In Fig. 1b and c, E_C, E_V, E_d, and E_U are, respectively, the conduction- and valence-band edges, the deep levels, and an upper state near the conduction band.)

2 Experiments

All samples were grown by molecular beam epitaxy. Sample A consists of 2488 Å of our GaAs deep centers, above which was a 1418 Å GaAs layer p-doped at $3.2 \times 10^{19}\,\mathrm{cm}^{-3}$. Sample B consists of 2974 Å of our GaAs deep centers, above which was no p-layer. Sample C consists of 2271 Å of our GaAs deep centers, above which was a 1294 Å GaAs layer p-doped at $2.5 \times 10^{19}\,\mathrm{cm}^{-3}$. The GaAs deep-center layers in samples A, B, and C were grown at 570 °C under As-rich conditions and high Si-dopant flux ($4.5 \times 10^{19}\,\mathrm{cm}^{-3}$). Sample D was a control sample of 21 periods of high-quality 120 Å InGaAs/120 Å InAlAs multiple quantum wells (MQWs) lattice matched to indium phosphide (InP). Sample E was a control sample of 2325 Å of bulk InGaAs lattice matched to InP. Samples A, B, and C were representative of several dozen growths. We chose to write about these specific samples because we had taken more comprehensive data

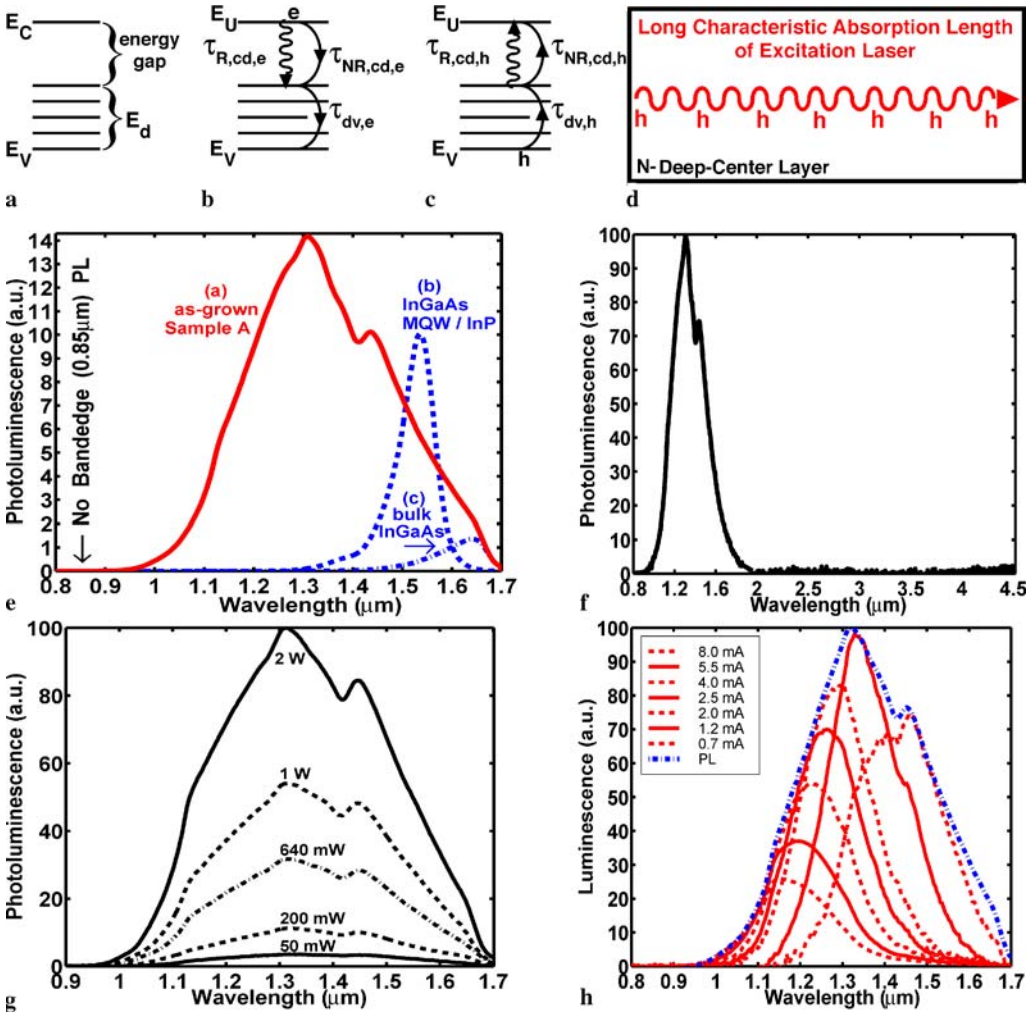

FIGURE 1 Energy levels and room-temperature PL. (**a**) Deep levels in n-GaAs. (**b**) Radiative and nonradiative lifetimes for electrons. (**c**) Radiative and nonradiative lifetimes for holes. (**d**) The excitation laser creates minority holes throughout the deep-center layer because the characteristic absorption length of the laser is greater than the deep-center-layer thickness. (**e**) PL from GaAs deep centers and from InGaAs. *Curve a* shows PL from GaAs deep centers in sample A. We calibrated the internal radiative efficiency of these GaAs deep centers to be over 90%. *Curve b* shows PL from the same thickness of high-quality InGaAs MQWs lattice matched to InP. (**f**) PL from GaAs deep centers over a wide wavelength range. (**g**) The room-temperature PL retains its spectral shape for all excitation laser peak powers up to 2 W. (**h**) PL spectrum (*dashed-dotted line*), on top of which is superimposed several normalized EL spectra (*solid* and *dashed lines*)

from these samples. Transmission, photoluminescence (PL), and Hall measurements were performed on samples A, B, and C. Electroluminescence (EL) and current–voltage were measured on samples A and C. PL was performed on samples D and E.

3 Results

Figure 1e shows room-temperature PL from GaAs deep centers and from InGaAs. The excitation in Fig. 1e and f was a 10 mW HeNe laser. All data was normalized to a sample thickness of 0.25 μm. Curve a in Fig. 1e shows PL from sample A of GaAs deep centers. Below, we estimate a deep-center internal radiative efficiency of over 90%. Curve b shows PL from sample D, the high-quality InGaAs/InAlAs MQWs on InP. Curve c shows PL from sample E, the bulk InGaAs on InP. The internal radiative efficiency was assessed in two ways (see the appendix). We found that the sample of as-grown GaAs deep centers (curve a in Fig. 1e) showed an internal radiative efficiency of 98%. Significantly, sample A showed a total PL (integrated over wavelength) greater than from the same thickness of both high-quality InGaAs MQWs lattice matched to InP (curve b in Fig. 1e) and bulk InGaAs (curve c in Fig. 1e).

Figure 1f shows room-temperature PL, obtained with a HeNe laser, from GaAs deep centers (sample A) over a wider wavelength range. Significantly, no PL is observed at the band edge (0.85 μm) (Figs. 1e, 1f, and 3b). In our n-type GaAs, this indicates an absence of free holes. The observed PL spectra are broad, and extend between 1.0 μm and 1.9 μm. These broad PL spectra result from transitions from states near the conduction band (E_U in Fig. 1b and c) to the many deep acceptors (Si_{Ga}-V_{Ga}, V_{Ga}, Si_{As}, Si_{Ga}-V_{Ga}-Si_{Ga}, and their ionization states) whose energies extend from the mid gap down to the valence band. Moreover, no PL is observed at wavelengths longer than 1.9 μm. The absence of long-wavelength transitions is consistent with an absence of deep-acceptor states (which act as both radiative and nonradiative paths) between the conduction band and mid gap. This absence of states is consistent with the observed large radiative efficiency (over 90%). Our observations indicate that holes created by the excitation laser relax quickly from the valence band to deep states near mid gap.

Figure 1g shows room-temperature PL from sample B as a function of the excitation peak power (50 mW, 200 mW, 640 mW, 1 W, and 2 W). The excitation was a 816 nm GaAs laser having a 700 μm × 200 μm spot size. Significantly, the shape of the PL spectra in Fig. 1g remains unchanged for all excitation intensities. Two peaks (at 1.31 μm and 1.45 μm) are always observed, and the relative heights of the two peaks remain unchanged for all excitation inten-

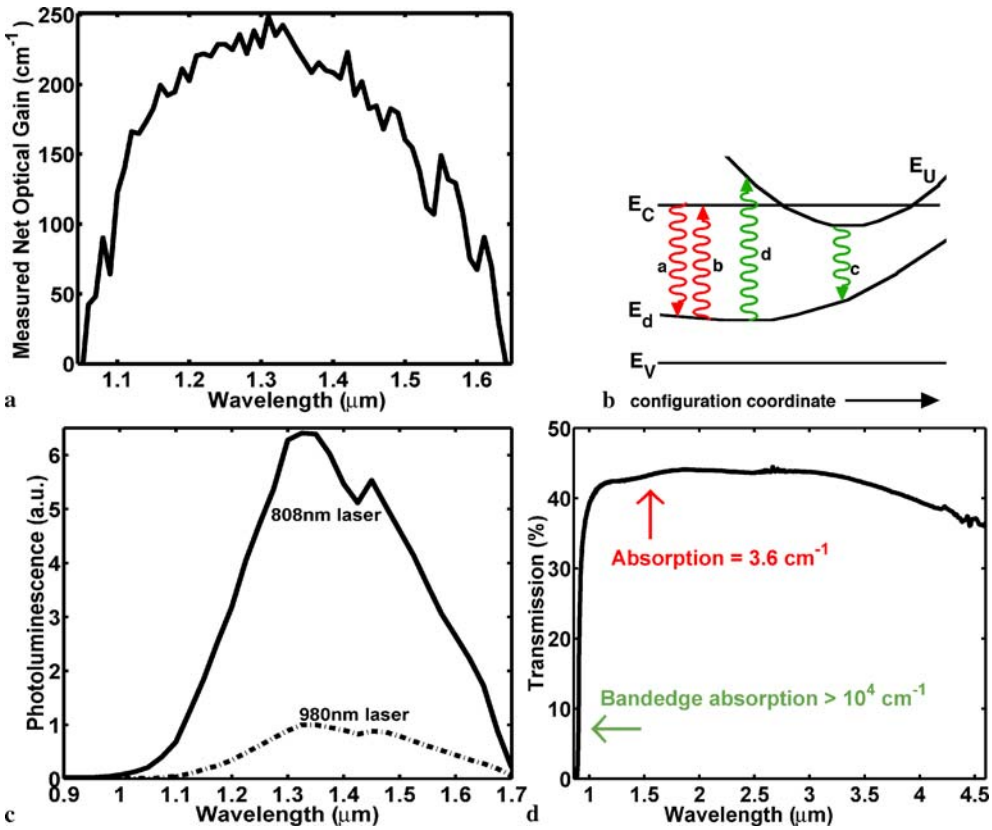

FIGURE 2 Gain and Franck–Condon shift. (**a**) Net optical gains[1] as high as 250 cm^{-1} were directly measured at 300 K from an epilayer of our novel GaAs deep centers for an injection of 1.4 kA/cm^2. (**b**) It is well known [15] that the donor–V_{Ga} complex shows a Franck–Condon shift. *Arrows c and d* show a Franck–Condon spectral shift of absorption away from luminescence. (**c**) PL from our GaAs deep centers at two different excitation wavelengths. The excitation at 808 nm (*solid curve*) yields much brighter PL than the excitation at 980 nm (*dashed curve*). All data correspond to the same number of incident photons. Thus, our novel material absorbs efficiently only at short wavelengths (< 980 nm), whereas the PL occurs at long wavelengths (1–1.7 μm). (**d**) The measured transmission through our GaAs deep centers indicates an absorption loss of 3.6 cm^{-1} at 1.6 μm wavelengths. Thus, at wavelengths (1–1.7 μm) of bright PL from our GaAs deep centers, the absorption loss is very small

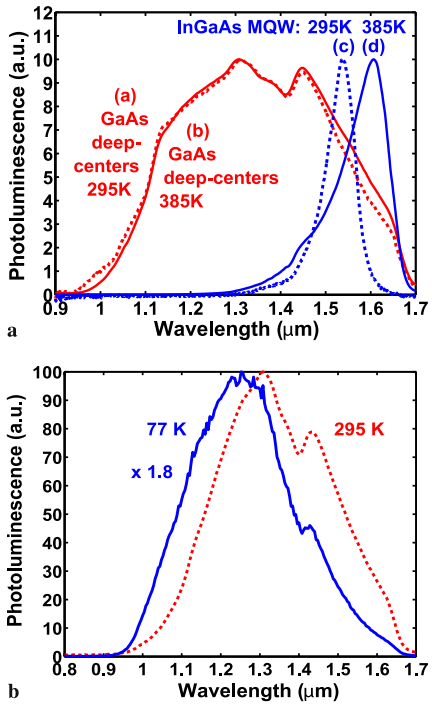

FIGURE 3 (**a**) The PL from GaAs deep centers and high-quality InGaAs MQWs at 295 K (*dashed lines*) and 385 K (*solid lines*). (**b**) The PL of GaAs deep centers at 295 K (*dashed line*) and 77 K (*solid line*). All PL have been normalized to the peak values. The PL at 77 K was 1.8 times that at room temperature (the PL efficiency at 295 K for the sample in Fig. 3b was less than 50%)

sities. Thus, even with a 2 W excitation (equivalent to 1.1 kW/cm^2), we were unable to saturate the deep-level transitions (so that the PL spectral shape changes with excitation).

In contrast, Fig. 1h (and Fig. 4a) shows that the EL changes significantly with injection. Figure 1h shows the PL spectrum (dashed-dotted line), on top of which is superimposed several EL spectra (solid and dashed lines), for sample C. The EL spectra have been normalized so that the EL peaks lie on top of the PL spectrum. Figure 1h shows that the EL at any specific current excites only a subset of the transitions (wavelengths) in the original PL spectrum. Moreover, as the current is incrementally increased, the EL spectrum shifts incrementally to shorter wavelengths. The latter indicates that the exact value of the current can be used to select specific transitions (wavelengths). The latter indicates inhomogeneous broadening of the PL.

The EL and PL in Fig. 1h are broad spectra rather than narrow lines. One reason is that, at these high doping concentrations, the impurities are in close proximity (~ 28 Å apart). Consequently, both the donor and compensating deep levels form energy bands rather than remain as atomically sharp energies.

Figure 2a shows that net optical gains[1] as high as 250 cm^{-1} were directly measured at 300 K from a 240 nm epilayer of our novel GaAs deep centers for an injection of 1.4 kA/cm^2. We used the variable stripe length method [30, 31] to measure gain with optical injection from a GaAs laser. For comparison, laser action in quantum dots [10] and InGaAsN [11] requires net gains of 14 cm^{-1} and 25 cm^{-1}, respectively. Thus, our novel material offers important new 1.3–1.5 μm wavelengths directly from the GaAs semiconductor without strained-lattice epitaxy.

It is well known [12, 25–29] that n-GaAs is compensated by donor–vacancy-on-gallium (donor–V_{Ga}) complexes under As-rich conditions. It is also well known [12, 15, 16, 20, 21] that the donor–V_{Ga} complex shows a Franck–Condon spectral shift of absorption away from luminescence, because V_{Ga} is highly coupled to the lattice. (Arrows a and b in Fig. 2b show absorption and luminescence at the same energies. Arrows c and d in Fig. 2b show a Franck–Condon shift where absorption occurs at higher energies than luminescence. The literature [15] says that the upper state E_U corresponds to a state centered on the donor in the donor–V_{Ga} complex, whereas the lower state E_d corresponds to a state centered on the V_{Ga} in the complex. Vacancies are highly coupled to lattice vibrations. The configuration coordinate in Fig. 2b describes the coupling of vacancies to lattice vibrations.) We now show that both transmission and photoluminescence at different excitation wavelengths are consistent with this well-known Franck–Condon shift.

Figure 2c shows the PL from our GaAs deep centers at two different excitation wavelengths. The excitation at 808 nm (solid curve) yields much brighter PL than the excitation at 980 nm (dashed curve). All data in Fig. 2c correspond to the same number of incident photons. The PL at different excitation wavelengths (i.e. photoluminescence excitation) is an often used measure of absorption. Thus, Fig. 2c shows that efficient absorption in our novel material occurs only at short wavelengths (< 980 nm), whereas the PL occurs at long wavelengths (1–1.7 μm). This is consistent with the well-known Franck–Condon shift associated with V_{Ga} complexes.

The measured transmission through our GaAs deep centers in Fig. 2d indicates an absorption loss of 3.6 cm^{-1} at 1.6 μm wavelength. This absorption loss of 3.6 cm^{-1} is four-orders-of-magnitude less than the typical band-edge absorption (10^4 cm^{-1}). Thus, the injection which achieves transparency in our novel material is four-orders-of-magnitude less than in direct-gap semiconductors. Figure 2d shows that, at wavelengths (1–1.7 μm) of bright PL from our GaAs deep centers, our material is nearly transparent even at zero injection. Figure 2d also shows that, in our novel material, absorption occurs at short wavelengths (< 1 μm), whereas the PL occurs at long wavelengths (1–1.7 μm). Again, this is consistent with the well-known Franck–Condon shift associated with V_{Ga} complexes. This Franck–Condon shift could become an important new paradigm for LEDs, lasers, and optical amplifiers operating at lower current.

It is well known that the PL from high-quality InGaAs MQWs changes dramatically with temperature. In stark contrast to InGaAs, we report virtually no change in both the spectral shape and peak height of the PL from our GaAs deep centers between 295 K (curve a in Fig. 3a) and 385 K (curve b in Fig. 3a). For comparison, the PL peak from high-quality InGaAs MQWs shifts from 1.53 μm to 1.60 μm between 295 K (curve c in Fig. 3a) and 385 K (curve d in Fig. 3a). This is accompanied by a drop (not shown) in the PL peak at 385 K to 0.7 times the PL peak at 295 K. This dramatic shift requires that fastidious attention be paid to the temperature stability of InGaAs MQW lasers. Figure 3b shows that the PL (normalized to the peak) from GaAs deep centers at 295 K (dashed line) will shift slightly to shorter wavelengths at 77 K (solid line). The PL at 77 K was 1.8 times that at room temperature.

Figure 4a shows room-temperature EL spectra from a p–n junction where the n-layer is our deep-center layer. The solid curve in Fig. 4b shows the meas-

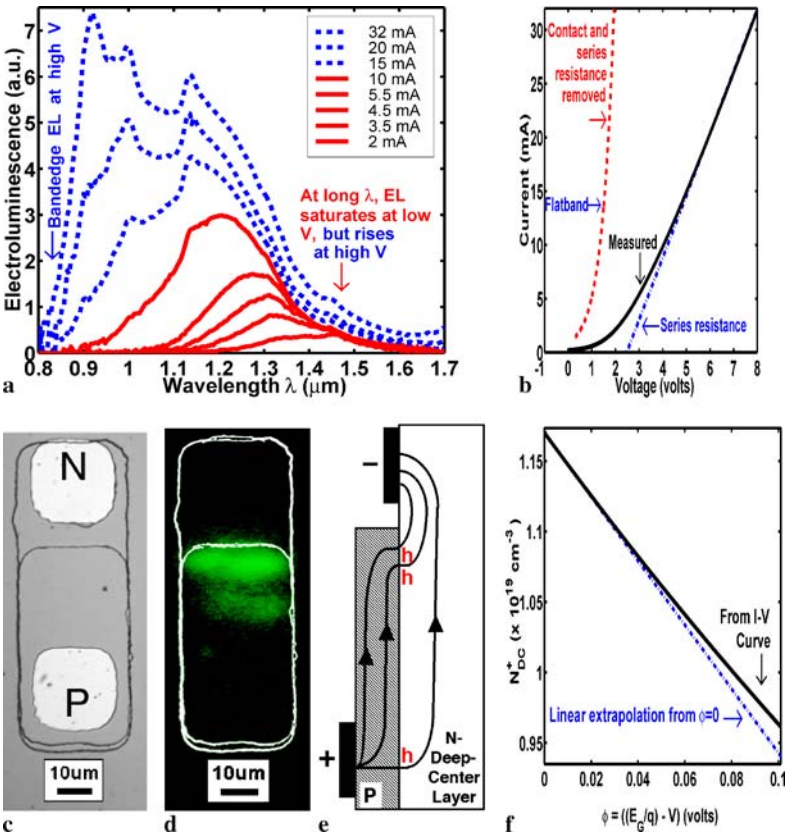

FIGURE 4 Electroluminescence. (**a**) Room-temperature EL spectra of p–n junction with the deep-center layer as the n-region. (**b**) The *solid curve* is the measured I–V curve of our device. The *dashed curve* is the same data with the TiAu contact diode and the series resistance (*dashed-dotted curve*) removed. (**c**) Our device consists of a 70 μm × 30 μm p-type top mesa and a 100 μm × 30 μm n-type bottom mesa. The contacts are 20 μm × 20 μm. (**d**) False-color image of the spatial distribution of the EL from the pixel surface. The brighter areas indicate more EL. (**e**) The spatial distribution of the current flow in a cross section of the fabricated devices. (**f**) The *solid curve* is the inferred concentration N_{DC}^{+} of deep centers which have captured holes on the n-side of the p–n junction as a function of the internal potential. The *dashed-dotted curve* is the slope of the *solid curve* at zero internal potential (flat band)

ured current–voltage (I–V) curve. By subtracting the TiAu contact (threshold of 1.0 V) from the applied voltage, the dashed-dotted curve in Fig. 4b shows that our device has a threshold of 1.4 V, as expected for GaAs. The dashed curve in Fig. 4b is the same data, with the TiAu contact and the series resistance (dashed-dotted curve) removed. Figure 4c shows a device structure. Figure 4d shows a false-color image of the observed EL. The brighter areas indicate more EL. Figure 4e explains why most of the observed EL comes from a 30 μm × 10 μm portion of the p-mesa closest to the n-contact. Since we found the p-layer to be twice as conducting as the n-layer, then, as the p–n junction is forward biased, twice as much of the lateral current flows through the p-layer as through the n-layer. The holes which comprise the current through the p-layer recombine with electrons only in that portion of the p-mesa closest to the n-contact. Figure 4f shows the concentration N_{DC}^{+} of deep centers which have captured a hole within one hole-diffusion length L_P of the p–n junction, as inferred from the dashed I–V curve of Fig. 4b and described in the appendix.

Details of the EL allow us to evaluate some important lifetimes in our material. We show below that the blue shift of the EL in Fig. 4a relative to the PL (Fig. 1) results from the small volume (one L_P into the deep-center layer) over which free holes exist in Fig. 4a. In the device shown in Fig. 5, which consists of only the n-type deep-center layer with no p-layer, holes are created over a large volume of the deep-center layer via impact ionization of high-energy majority electrons all along the electron paths. When the holes are created over a large volume of the deep-center layer (Fig. 5a), the EL spectral shape (Fig. 5b) looks a lot like the PL (Fig. 1). In PL, holes are also created over a large volume (the entire deep-center layer). (This is indicated in Fig. 1d by an epilayer thickness which was always less than the characteristic absorption length of the excitation laser in PL.)

Figures 5 and 3a show that the blue shift of the EL in Fig. 4a cannot be explained by either device heating or a Stark effect due to an internal electric field. The voltage and current used for electron injection to obtain the EL in Fig. 5b are somewhat larger than those used in the p–n junction EL of Fig. 4a. This is significant because any I–V heating would be greater in Fig. 5 than in Fig. 4a. Moreover, the electric field across the deep-center layer (and any Stark effect) is greater in Fig. 5 (15 V drop) than in Fig. 4a ($8 - 2.5 = 5.5$ V drop). Since the EL in Figs. 5b and 4a incur similar I-V heating and internal electric field (and Stark effect), then heating and electric field (and Stark effect) cannot explain the spectral blue shift in the p–n junction EL of Fig. 4a relative to the EL of Fig. 5b and to the PL of Fig. 1. This is consistent with our earlier observation in Fig. 3a that the PL at 385 K is virtually the same as the PL at 295 K.

Significantly, no band-edge (0.85 μm) PL is observed in Figs. 1e, f, and 3b. The absence of band-edge PL from the n-type deep-center layer indicates that holes are quickly trapped by deep centers before a conduction-to-valence-band transition occurs. The hole capture $\tau_{dv,h}$ into a deep center is indicated in Fig. 1c. The hole-diffusion length L_P is related to $\tau_{dv,h}$ through

$$L_P^2 = (k_B T/q)\, \mu_h\, \tau_{dv,h}\,,$$

where μ_h is the hole mobility in the deep-center layer. A fast $\tau_{dv,h}$ implies a short L_P. This has important consequences for EL. Figure 6a shows that the electrically injected holes from the p-region are immediately captured by deep centers in the first L_P of the n-type deep-center layer. This causes an accumulation of positive charge in the first L_P of the n-layer. Figure 6b shows that the band bending of Fig. 6c results from both holes trapped on deep centers, as well as the well-known p–n junction depletion charge.

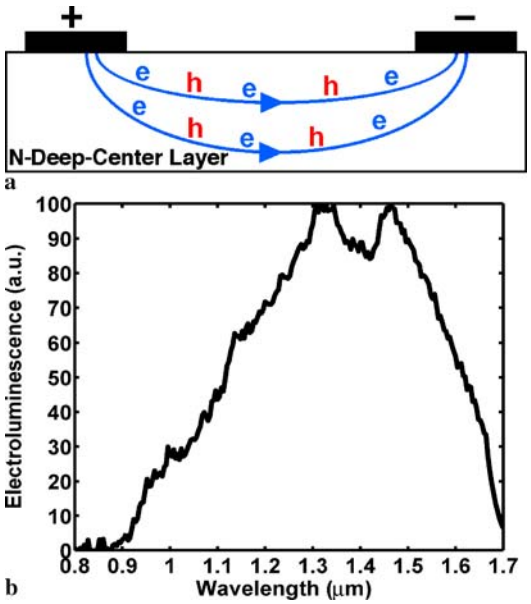

FIGURE 5 Room-temperature EL from a device which does not have a p-layer. (**a**) In a device consisting of only the n-type deep-center layer, holes are created via impact ionization of electrons over a large volume of the deep-center layer (all along the electron paths). (**b**) The EL spectra from the deep-center layer look a lot like the PL when the holes are created in a large volume of the deep-center layer (all along the electron paths). (The applied voltage was 15 V at 50% duty cycle and the electron-injection current was 62 mA.) This is unlike Fig. 4a, where the EL spectra exhibit a blue shift relative to the PL and where the holes in Fig. 4a exist only in a small volume (within the first L_P) of the deep-center layer

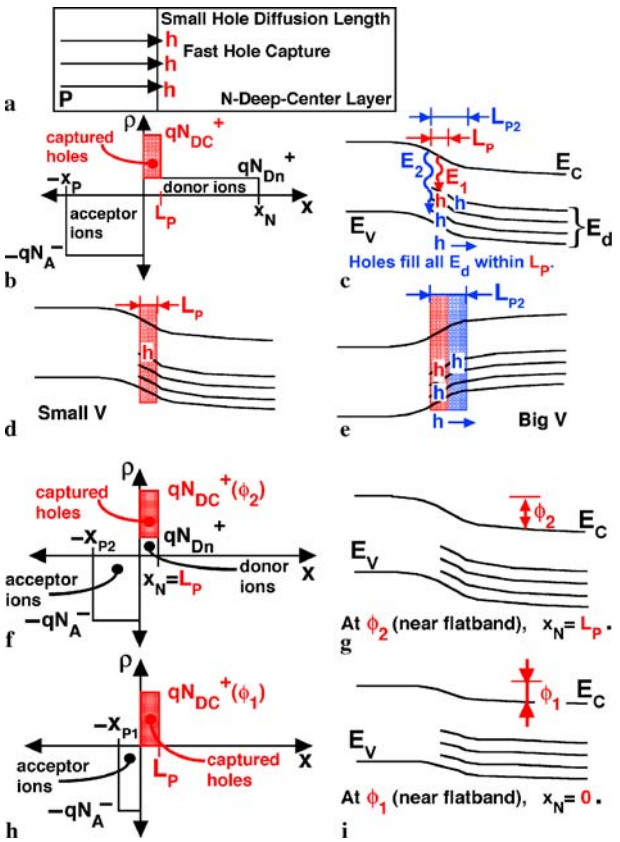

FIGURE 6 Hole capture into deep levels. (**a**) The electrically injected holes from the p-region are immediately captured within the first L_P of the n-type deep-center layer. (**b**) Charges associated with the p–n junction. (**c**) The energy-band diagram of the p–n junction. (**d**) As the injected holes are captured, positive charge accumulates within the first L_P of the deep-center layer. (**e**) At higher currents, holes have filled up most of the deep levels within one L_P of the deep-center layer. Thus, within one L_P of the deep-center layer, some free holes exist and can participate in band-edge emission. These free holes are captured within L_{P2} of the deep-center layer. (**f**) Charge associated with both depletion and hole capture, when the depletion width x_N equals L_P. (**g**) φ_2 (near flat band) is defined when the depletion width x_N equals L_P. (**h**) Charge associated with both depletion and hole capture at a voltage near flat band where $x_N = 0$. Here, the charge in the n-GaAs results solely from hole capture into deep levels N_{DC}^{+}. (**i**) φ_1 (near flat band) is defined when the depletion width $x_N = 0$

Careful scrutiny of the EL in Fig. 4a indicates a small fixed value of L_P. The solid curves in Fig. 4a show that the EL at longer than 1.35 μm increases for small injections, but saturates at a low current. For example, the EL at 1.45 μm in Fig. 4a remains the same for all injections between 2 mA and 10 mA. This saturation of the EL brightness at long wavelengths can be explained by a small value of L_P and the small number of deep centers within a small L_P. As the current is increased, holes fill all high-energy deep levels (near mid gap) within one L_P of the junction, as shown in Fig. 6d. At higher injection, holes then populate lower deep levels (closer to the valence band) within one L_P of the junction. This makes possible transitions involving higher photon energy (E_2 as well as E_1 in Fig. 6c), as electrons combine with holes trapped at deep levels closer to the valence band. Thus, at higher injection, the EL spectra in Fig. 4a shift to shorter wavelengths.

At currents greater than 10 mA (dashed line in Fig. 4a), the EL at longer than 1.35 μm, surprisingly, starts to rise again. This increase in the long-wavelength EL is accompanied by the presence of free holes: band-edge (0.85 μm) EL is observed only for injections greater than 10 mA in Fig. 4a. This is sensible because, when most deep centers within one L_P of the junction have captured a hole, the repulsive Coulomb force makes it difficult for additional holes to be captured by the same deep centers. Thus, at these higher currents, some free holes exist within one L_P of the junction (Fig. 6c and e), and these free holes can give rise to band-edge EL. The latter holes can also be trapped into unoccupied deep states near mid gap further ($L_{P2} > L_P$ in Fig. 6c and e) from the junction. This explains why band-edge EL (dashed curves in Fig. 4a) occurs simultaneously with a sudden rise in EL at 1.35–1.45 μm beyond the saturated values at low current.

Thus, at an injection ∼ 15 mA, most of the deep centers (Si_{Ga}-V_{Ga}) within one L_P of the junction have captured one hole. (If we assume that fewer deep centers within this first L_P have captured one hole, then N_{DC}^{+} would be smaller than the value concluded below. This would imply an Einstein B coefficient even larger than the value concluded below.) From the literature

[27–29], when the total Si in GaAs is $4.5\times10^{19}\,\mathrm{cm}^{-3}$, $\mathrm{Si_{Ga}}$-$\mathrm{V_{Ga}}$ is observed to be $\sim 1.5\times10^{19}\,\mathrm{cm}^{-3}$. Thus, at 15 mA in Fig. 4a, N^{+}_{DC} is $\sim 1.5\times10^{19}\,\mathrm{cm}^{-3}$. This observation allows us to relate the ordinate axis (current) in Fig. 4b to the ordinate axis (N^{+}_{DC}) in Fig. 4f.

The appendix shows how L_P, $\tau_{dv,h}$, $\tau_{cd,h}$, and the Einstein B_{cd} coefficient can be estimated for the device in Fig. 4a. The PL of the deep levels in Fig. 4a showed an internal radiative efficiency η of 16%. L_P and $\tau_{dv,h}$ can be found by evaluating that internal potential (φ_1 in Fig. 6h and i) across the junction when the depletion charge in the p-GaAs equals just the hole charge trapped on deep centers. The hole lifetime in deep levels $\tau_{cd,h}$ can be found by equating the injection current to the recombination flux. The Einstein B_{cd} can be found from $\tau_{cd,h}$ and η. The result is that $\tau_{dv,h}=15$ fs, $\tau_{cd,h}=130$ ps, and $B_{cd}=8.2\times10^{-10}\,\mathrm{cm}^3/\mathrm{s}$.

We now compare our numbers with the literature on hole trapping onto deep acceptors. Figure 4a shows that many deep levels exist just above the valence-band edge, and these levels quickly trap free holes. Pump–probe experiments show a lifetime of 100 fs for hole trapping on $\mathrm{V_{Ga}}$ [32, 33], and this 100 fs is in good agreement with our $\tau_{dv,h}$. Our fast hole capture $\tau_{dv,h}$ is consistent with our observed difficulty in photoetching.

Our estimate of the Einstein B coefficient $B_{cd}=8.2\times10^{-10}\,\mathrm{cm}^3/\mathrm{s}$ for our novel GaAs material is larger than the B coefficient [3, 34–36] of $10^{-10}\,\mathrm{cm}^3/\mathrm{s}$ for the conduction-to-valence-band transition in InGaAsP. This is reasonable because, as mentioned with respect to Fig. 2b, the upper state of our optical transition is most likely a deep-center (probably $\mathrm{Si_{Ga}}$-$\mathrm{V_{Ga}}$) bound state, rather than a conduction-band state. Optical transitions between deep-center bound states are likely to be stronger than the conduction-to-valence-band transition. The appendix uses realistic numbers to estimate B_{cd}. However, even if our estimate is too optimistic by a factor of seven, our B_{cd} would still be larger than the B coefficient in InGaAsP. Our larger Einstein B coefficient explains why the observed radiative efficiency and optical gain in our novel material are greater than in conventional direct-gap materials at 1.3–1.5 μm wavelengths. Thus, our new material is an ideal four-level system, with a large Einstein B coefficient and fast depopulation of (fast fs hole capture into) the lower state of optical emission.

ACKNOWLEDGEMENTS We acknowledge discussions with R.K. Chang, ONR Grant No. N00014-04-1-0486, and NSF Grant Nos. ECS-0134056 and DMR-0520495.

Appendices

A Two measurements of radiative efficiency

The internal radiative efficiency was assessed in two ways. First, our measured PL were compared with our brightest samples of p-GaAs (200 nm of beryllium (Be)-doped GaAs at $4\times10^{19}\,\mathrm{cm}^{-3}$). The PL efficiency of p-GaAs is well known [37–40]. Second, we directly measured the PL which is captured by a F/1.5 lens, and focussed onto a calibrated photodetector with a F/4 lens. We assumed that the externally measured PL consists [41, 42] of only that portion of the internal PL radiation which is incident upon the sample surface at less than the critical angle.

B Estimate of L_P

At small biases, the depletion charge is much larger than the hole charge trapped on deep centers within one L_P of the junction. At these biases, the depletion width x_N in the n-type deep-center layer is much greater than L_P. This is shown in Fig. 6b. At a voltage near flat band, the depletion width x_N has been reduced to L_P. At this voltage, the internal potential, defined as φ_2, is found by equating the depletion charge in the p-GaAs to the sum of the depletion charge in the n-GaAs and the hole charge trapped on deep centers. This is indicated in Fig. 6f and g. At an even higher voltage, which is even closer to flat band, the depletion width x_N has been reduced to zero. At this voltage, the internal potential, defined as φ_1, is found by equating the depletion charge in the p-GaAs to the hole charge trapped on deep centers in the n-GaAs. This is shown in Fig. 6h and i. If we equate the depletion charge, $qN^{-}_{\mathrm{A}}x_{P1}$, in the p-GaAs to the hole charge, $qN^{+}_{\mathrm{DC}}(\varphi_1)L_P$, trapped on deep centers, then the equations of an abrupt depletion model determine L_P in terms of φ_1:

$$L_P=[2\varepsilon/q]^{\frac{1}{2}}\varphi_1^{\frac{1}{2}}\left[N^{-}_{\mathrm{A}}+N^{+}_{\mathrm{DC}}(\varphi_1)\right]^{-\frac{1}{2}}\times\left[N^{-}_{\mathrm{A}}/N^{+}_{\mathrm{DC}}(\varphi_1)\right]^{\frac{1}{2}}.$$

C Internal potential resulting from trapped holes

From above, φ_2 is defined as the internal potential for which the depletion charge, $qN^{-}_{\mathrm{A}}x_{P2}$, in the p-GaAs is equal to the sum of the depletion charge in the n-GaAs, $qN^{+}_{Dn}L_P$, and the hole charge, $qN^{+}_{\mathrm{DC}}(\varphi_2)L_P$, trapped on deep centers:

$$\varphi_2=[q/2\varepsilon]\left[N^{+}_{\mathrm{DC}}(\varphi_2)+N^{+}_{Dn}\right]L_P^2\times\left[1+\left(\left\{N^{+}_{\mathrm{DC}}(\varphi_2)+N^{+}_{Dn}\right\}/N^{-}_{\mathrm{A}}\right)\right].$$

Similarly,

$$\varphi_1=[q/2\varepsilon]N^{+}_{\mathrm{DC}}(\varphi_1)L_P^2\times\left[1+(N^{+}_{\mathrm{DC}}(\varphi_1)/N^{-}_{\mathrm{A}})\right].$$

If the p-GaAs is much more highly doped than the n-GaAs, then

$$N^{-}_{\mathrm{A}}\gg N^{+}_{\mathrm{DC}}(\varphi_2)+N^{+}_{Dn}$$

and

$$N^{-}_{\mathrm{A}}\gg N^{+}_{\mathrm{DC}}(\varphi_1).$$

The latter imply that

$$(\varphi_2/\varphi_1)\simeq\left[N^{+}_{\mathrm{DC}}(\varphi_2)+N^{+}_{Dn}\right]/N^{+}_{\mathrm{DC}}(\varphi_1).$$

We find that $N^{+}_{\mathrm{DC}}(\varphi_1)$ can be accurately related to φ_1 through

$$N^{+}_{\mathrm{DC}}(\varphi_1)=a_0+a_1\varphi_1+a_2\varphi_1^2,$$

where the a_i are found from a fit to the measured I–V curve. For small values of φ_1 and φ_2, the self-consistent solution for φ_1 and φ_2 satisfies

$$(\varphi_2/\varphi_1)=c_1+c_2\varphi_1+c_3\varphi_1^2+c_4\varphi_1^3.$$

Using these expansions of N^{+}_{DC} and (φ_2/φ_1), the self-consistent solution for φ_1 and φ_2 is found to satisfy

$$c_2=c_4=0,\quad c_1=1+(N^{+}_{Dn}/a_0),$$
$$c_3=a_2c_1(c_1-1)/a_0,\quad\text{and}$$
$$a_2c_3\varphi_1^4\left[(2c_1-1)+c_3\varphi_1^2\right]=0.$$

In the last equation, the term in the square brackets is greater than zero for

all real φ_1, and thus φ_1 must satisfy: either

$$[\varphi_1 = 0 \quad \text{for} \quad a_2 \neq 0] \,, \quad \text{or}$$
$$[a_2 = 0 \quad \text{for} \quad \varphi_1 \neq 0] \,.$$

The first solution says that, in the general case in which $N^+_{\mathrm{DC}}(\varphi_1)$ has a nonzero a_2 (quadratic) term, the only self-consistent solution is $\varphi_1 = \varphi_2 = 0$. However, this implies that $L_P = 0$, which is too crude an approximation. The second solution yields a better approximation for L_P. This second solution says that, in the general case of a nonzero solution φ_1, $N^+_{\mathrm{DC}}(\varphi_1)$ must be purely linear in the neighborhood of φ_1 (i.e. $a_2 = 0$). Thus, at the physically significant φ_2, where the depletion width x_N equals L_P, the $N^+_{\mathrm{DC}}(\varphi_2)$ curve must be purely linear in φ_2. Figure 4f shows that the N^+_{DC} (φ_2) curve is purely linear in φ_2 when $\varphi_2 < 0.03\,\mathrm{V}$. By including the terms in $N^+_{\mathrm{DC}}/N^-_{\mathrm{A}}$, a more precise numerical solution is found to be $\varphi_1 = 0.03\,\mathrm{V}$. Assuming that $\varphi_1 = 0.03\,\mathrm{V}$ and $N^-_{\mathrm{A}} = 6 \times 10^{19}\,\mathrm{cm}^{-3}$ for the p-region of the device in Fig. 4, $N^+_{\mathrm{DC}}\,(\varphi_1) = 1.1 \times 10^{19}\,\mathrm{cm}^{-3}$ from Fig. 4f, and $\mu = 84\,\mathrm{cm}^2/\mathrm{V\,s}$ (typical of our highly doped p-GaAs), then L_P and $\tau_{dv,h}$ are calculated to be, respectively, 18 Å and 15 fs. L_P is unlikely to be much larger, because φ_1 must be near zero (flat band).

D Estimate of $\tau_{cd,h}$

At a large enough current, I_{IN}, when each deep center within one L_P of the junction has captured one hole, the total number of holes trapped on deep centers is $N^+_{\mathrm{DC}} A L_P$, where N^+_{DC} is the concentration of deep centers which have captured at least one hole, and A is the area of the device. If $\tau_{cd,h}$ is the lifetime for a hole in a deep level to be captured into E_{U} near the conduction band (i.e. an electron to make a transition from E_{U} to a deep level), then, in the steady state, I_{IN} must supply the total recombination flux $qN^+_{\mathrm{DC}} A L_P/\tau_{cd,h}$. The recombination velocity $L_P/\tau_{cd,h}$ of holes in the deep-center layer is then

$$(L_P/\tau_{cd,h}) = \left[I_{\mathrm{IN}}/(qN^+_{\mathrm{DC}}A)\right] \,.$$

The lifetime $\tau_{cd,h}$ of holes in deep levels is related to the lifetimes in Fig. 1c through

$$\tau^{-1}_{cd,h} = \tau^{-1}_{R,cd,h} + \tau^{-1}_{NR,cd,h} \,.$$

Earlier, we mentioned that 15 mA in Fig. 4a corresponds to $N^+_{\mathrm{DC}} = 1.5 \times 10^{19}\,\mathrm{cm}^{-3}$. Assuming that $L_P = 18$ Å, $A = 30\,\mu\mathrm{m} \times 10\,\mu\mathrm{m}$, $N^+_{\mathrm{DC}} = 1.5 \times 10^{19}\,\mathrm{cm}^{-3}$, and $I_{\mathrm{IN}} = (2/3) \times 15\,\mathrm{mA}$ (where the '2/3' arises because only 2/3 of the current flows laterally through the p-layer and then through the area A), we calculate $\tau_{cd,h} = 130\,\mathrm{ps}$.

E Estimate of B_{cd}

If N^+_{Dn} is the net donor (total donor minus total acceptor) concentration in the deep-center layer, then N^+_{Dn} equals the free-electron concentration in the n-type deep-center layer. Hall measurements of the sample used in Fig. 4 show that $N^+_{Dn} = 1.5 \times 10^{18}\,\mathrm{cm}^{-3}$. The Einstein B coefficient [3] B_{cd} can be found by equating the two expressions for the radiative flux, $B_{cd} N^+_{Dn} p$ and $p/\tau_{R,cd,h}$:

$$B_{cd} = 1/(N^+_{Dn}\tau_{R,cd,h}) \,,$$

where $\eta_{cd} = (\tau_{cd,h}/\tau_{R,cd,h})$. Assuming that $\tau_{cd,h} = 130\,\mathrm{ps}$ and $\eta_{cd} = 16\%$ for the device in Fig. 4a, we calculate $B_{cd} = 8.2 \times 10^{-10}\,\mathrm{cm}^3/\mathrm{s}$.

REFERENCES

1 M.G. Bernard, G. Duraffourg, Phys. Stat. Solidi **1**, 699 (1961)
2 A. Yariv, *Quantum Electronics*, 2nd edn. (Wiley, New York, 1975)
3 G.P. Agrawal, N.K. Dutta, *Long-wavelength Semiconductor Lasers* (Van Nostrand Reinhold, New York, 1986)
4 R.N. Hall, G.E. Fenner, J.D. Kingsley, T.J. Soltys, R.O. Carlson, Phys. Rev. Lett. **9**, 366 (1962)
5 M.I. Nathan, W.P. Dumke, G. Burns, F.H. Dills, G. Lasher, Appl. Phys. Lett. **1**, 62 (1962)
6 T.M. Quist, R.J. Keyes, W.E. Krag, B. Lax, A.L. McWhorter, R.H. Rediker, H.J. Zeiger, Appl. Phys. Lett. **1**, 91 (1962)
7 N. Holonyak Jr., S.F. Bevacqua, Appl. Phys. Lett. **1**, 82 (1962)
8 W. Ha, V. Gambin, M. Wistey, S. Bank, H. Yuen, S. Kim, J.S. Harris, Electron. Lett. **38**, 277 (2002)
9 R. Shau, H. Halbritter, F. Riemenschneider, M. Ortsiefer, J. Rosskopf, G. Bohm, M. Maute, P. Meissner, M.-C. Amann, Electron. Lett. **39**, 1728 (2003)
10 D.R. Matthews, H.D. Summers, P.M. Smowton, M. Hopkinson, Appl. Phys. Lett. **81**, 4904 (2002)
11 M. Hofmann, A. Wagner, C. Ellmers, C. Schlichenmeier, S. Schaefer, F. Hoehnsdorf, J. Koch, W. Stolz, S.W. Koch, W.W. Ruehle, J. Hader, J.V. Moloney, E.P. O'Reilly, B. Borchert, A.Yu. Egorov, H. Riechert, Appl. Phys. Lett. **78**, 3009 (2001)
12 H. Lei, H.S. Leipner, V. Bondarenko, J. Schreiber, J. Phys.: Condens. Matter **16**, S279 (2004)
13 M. Tajima, R. Toba, N. Ishida, M. Warashina, Mater. Sci. Technol. **13**, 949 (1997)
14 J. Kanga, K. Hoshikawaa, M. Tajima, T. Fukudaa, J. Cryst. Growth **135**, 623 (1994)
15 E.W. Williams, Phys. Rev. **168**, 922 (1968)
16 M.A. Reshchikov, A.A. Gutkin, V.E. Sedov, Mater. Sci. Forum **196–201**, 237 (1995)
17 M. Suezawa, A. Kasuya, Y. Nishina, K. Sumino, J. Appl. Phys. **69**, 1618 (1991)
18 J.K. Kung, W.G. Spitzer, J. Appl. Phys. **45**, 4477 (1974)
19 S.Y. Chiang, G.L. Pearson, J. Luminesc. **10**, 313 (1975)
20 T. Sauncy, C.P. Palsule, M. Holtz, S. Gangopadhyay, S. Massie, Phys. Rev. B **53**, 1900 (1996)
21 M. Suezawa, A. Kasuya, Y. Nishina, K. Sumino, J. Appl. Phys. **76**, 1164 (1994)
22 F.M. Vorobkalo, K.D. Glinchuk, A.V. Prokhorovich, G. John, Phys. Stat. Solidi A **15**, 287 (1973)
23 F.M. Vorobkalo, K.D. Glinchuk, A.V. Prokhorovich, Phys. Stat. Solidi A **7**, 135 (1971)
24 F.M. Vorobkalo, K.D. Glinchuk, A.V. Prokhorovich, Phys. Stat. Solidi A **1**, K109 (1970)
25 P. Ebert, Curr. Opin. Solid State Mater. Sci. **5**, 211 (2001)
26 J. Gebauer, M. Lausmann, T.E.M. Staab, R. Krause-Rehberg, M. Hakala, M.J. Puska, Phys. Rev. B **60**, 1464 (1999)
27 C. Domke, P. Ebert, K. Urban, Phys. Rev. B **57**, 4482 (1998)
28 C. Domke, P. Ebert, M. Heinrich, K. Urban, Phys. Rev. B **54**, 10 288 (1996)
29 J. Gebauer, R. Krause-Rehberg, C. Domke, P. Ebert, K. Urban, Phys. Rev. Lett. **78**, 3334 (1997)
30 K.L. Shaklee, R.E. Nahory, R.F. Leheny, J. Luminesc. **7**, 284 (1973)
31 K.L. Shaklee, R.F. Leheny, Appl. Phys. Lett. **18**, 475 (1971)
32 M.R. Melloch, J.M. Woodall, E.S. Harmon, N. Otsuka, F.H. Pollak, D.D. Nolte, R.M. Feenstra, M.A. Lutz, Ann. Rev. Mater. Sci. **25**, 547 (1995)
33 M.R. Melloch, D.D. Nolte, J.M. Woodall, J.C.P. Chang, E.S. Harmon, Crit. Rev. Solid State Mater. Sci. **21**, 189 (1996)
34 R. Olshansky, C. Su, J. Manning, W. Powazinik, IEEE J. Quantum Electron. **QE-20**, 838 (1984)
35 E. Wintner, E.P. Ippen, Appl. Phys. Lett. **44**, 999 (1984)
36 T. Uji, K. Iwamoto, R. Lang, IEEE Trans. Electron Devices **ED-30**, 316 (1983)
37 H. Ito, T. Furuta, T. Ishibashi, Appl. Phys. Lett. **58**, 2936 (1991)
38 H.C. Casey Jr., F. Stern, J. Appl. Phys. **47**, 631 (1976)
39 R.J. Nelson, R.G. Sobers, J. Appl. Phys. **49**, 6103 (1978)
40 A. Maassdorf, S. Gramlich, E. Richter, F. Brunner, M. Weyers, G. Traenkle, J.W. Tomm, Y.I. Mazur, D. Nickel, V. Malyarchuk, T. Guenther, C. Lienau, A. Baerwolff, T. Elsaesserm, J. Appl. Phys. **91**, 5072 (2002)
41 E. Yablonovitch, G. Cody, IEEE Trans. Electron Devices **ED-29**, 300 (1982)
42 E. Yablonovitch, J. Opt. Soc. Am. **72**, 899 (1982)